Photochemistry and Photobiology, 2014, 90: 596–608

Photodamage in a Mitochondrial Membrane Model Modulated by the Topology of Cationic and Anionic *Meso*-Tetrakis Porphyrin Free Bases

Cintia Kawai[†1], Juliana C. Araújo-Chaves[†1], Taciana Magrini[1], Camila O. C. C. Sanches[1], Sandra M. S. Pinto[1], Herculano Martinho[1], Nasser Daghastanli[2] and Iseli L. Nantes[*1]

[1]Centro de Ciências Naturais e Humanas (CCNH), Universidade Federal do ABC, Santo André, SP, Brazil
[2]Centro de Engenharia, Modelagem e Ciências Sociais Aplicadas (CECS), Universidade Federal do ABC, Santo André, SP, Brazil

Received 20 May 2013, accepted 9 December 2013, DOI: 10.1111/php.12228

ABSTRACT

The photodynamic effects of the cationic TMPyP (*meso*-tetrakis [*N*-methyl-4-pyridyl]porphyrin) and the anionic TPPS4 (*meso*-tetrakis[4-sulfonatophenyl]porphyrin) against PC/CL phosphatidylcholine/cardiolipin (85/15%) membranes were probed to address the influence of phorphyrin binding on lipid damage. Electronic absorption spectroscopy and zeta potential measurements demonstrated that only TMPyP binds to PC/CL large unilamellar vesicles (LUVs). The photodamage after irradiation with visible light was analyzed by dosages of lipid peroxides (LOOH) and thiobarbituric reactive substance and by a contrast phase image of the giant unilamellar vesicles (GUVs). Damage to LUVs and GUVs promoted by TMPyP and TPPS4 were qualitatively and quantitatively different. The cationic porphyrin promoted damage more extensive and faster. The increase in LOOH was higher in the presence of D_2O, and was impaired by sodium azide and sorbic acid. The effect of D_2O was higher for TPPS4 as the photosensitizer. The use of DCFH demonstrated that liposomes prevent the photobleaching of TMPyP. The results are consistent with a more stable TMPyP that generates long-lived singlet oxygen preferentially partitioned in the bilayer. Conversely, TPPS4 generates singlet oxygen in the bulk whose lifetime is increased in D_2O. Therefore, the affinity of the porphyrin to the membrane modulates the rate, type and degree of lipid damage.

INTRODUCTION

Photodynamic therapy (PDT) is a noninvasive therapeutic method mainly used in the fields of dermatology, otorhinolaryngology, ophthalmology, neurology, gastroenterology and urology for the treatment of precancerous and superficial malignant skin tumors as well as degenerated and infected tissues (1–3). The photosensitization is achieved by electronically exciting a dye photosensitizer (PS) promoted by the absorption of light at suitable wavelength (4–7). The photodynamic action can be performed directly with the triplet excited state of the dye and/or with $O_2(^1\Delta_g)$ (singlet oxygen) generated by electronic excitation energy transfer, that is by Type-I and/or Type-II mechanisms, respectively (4–7). The selectivity of PDT constitutes an advantage comparatively to traditional methods, such as chemotherapy and radiotherapy (8–10), due to its selective and localized actions (11,12). A high efficiency of PDT with minimal side effects depends on some chemical and physical characteristics of the PS: (1) highest affinity for the diseased cells or the pathogenic organisms; (2) low toxicity in the dark; (3) chemical stability and low aggregation; (4) rapid body clearance; (5); high quantum yields of a long-lived excited triplet state and (6) electronic absorption at wavelengths of maximum transparence of biological tissues, avoiding the absorption of endogenous chromophores, such as melanin, hemoglobin and cytochromes and enabling deeper light penetration (13,14). However, wavelengths longer than 900 nm should be avoided because of their insufficient energy to excite a dye to the triplet state (12,15,16).

A diversity of PS compounds satisfies the above-mentioned desirable characteristics, and includes the porphyrins (17,18). The absorption spectra of porphyrins in the visible region includes the therapeutic window for PS compounds (17,18) The uptake and localization of a PS in cells depends on its chemical structure, the mechanism of its uptake by the cell, its intrinsic affinity to cell components and any chemical modifications in the course of irradiation (19–21).

Biological and synthetic porphyrins are both largely used as PS in PDT. Studies about the biological effects of two *meso*-tetrakis porphyrins, TPPS4 (anionic) and TMPyP (cationic) demonstrated that the cationic porphyrin has affinity to the inner mitochondrial membrane (22,23). Therefore, in mitochondria, manganese TMPyP has been used as an antioxidant against superoxide ions and as a prooxidant agent in the corresponding ferric form (21,24–26). However, cationic TMPyP has been found also in lysosomes and the nucleus, and, after irradiation, both TMPyP and TPPS4 have been found preferentially in the nucleus, probably due to their association with proteins that migrate to the nucleus after oxidation (21,27).

Biological membranes are targets for the action of PDT. Therefore, numerous studies have been concerned with the interaction of porphyrins with liposomes and other membrane mimetic models (28–34). However, literature lacks comparative studies involving photodynamic action of hydrophilic porphyrins on mitochondrial membrane models. The PDT action on biological membranes directly contributes to cell death due to local oxidative damages

*Corresponding author emails: ilnantes@gmail.com and ilnantes@ufabc.edu.br (Iseli L. Nantes)
†These authors contributed equally

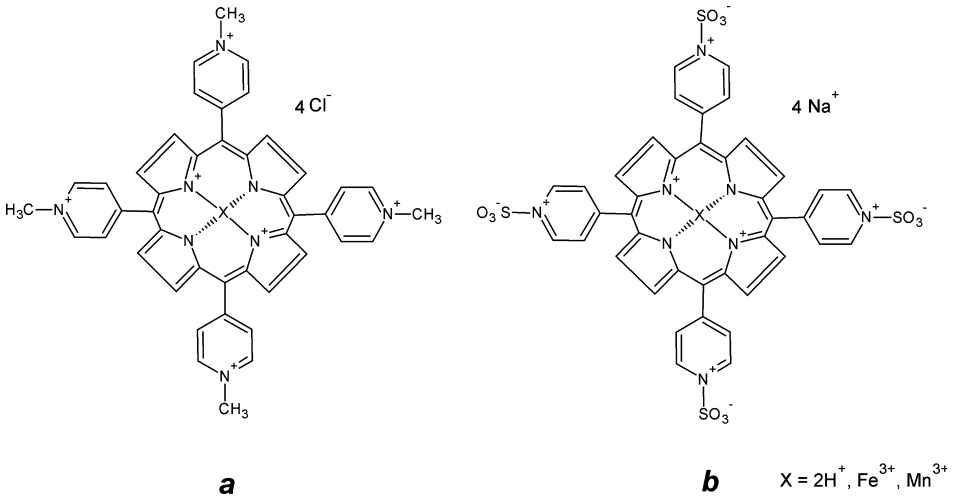

Chart 1. Structures of TMPyP and TPPS4: *a*-cationic TMPyP (*meso*-tetrakis (*N*-methyl-4-pyridyl)porphyrin). *b*-anionic TPPS4 (*meso*-tetrakis(4-sulfonatophenyl)porphyrin)

and by secondary signaling death pathways. Mitochondria are commonly involved in the apoptosis promoted by PDT by accumulating the PS or by activating the intrinsic apoptotic pathway as a consequence of damages to other cell structures (35,36). Therefore, it is relevant to understand the correlation of the porphyrin binding to mitochondrial membranes with their photodynamic effects. This study investigated the photodynamic action of the cationic TMPyP (*meso*-tetrakis [*N*-methyl-4-pyridyl]porphyrin) and the anionic TPPS4 (*meso*-tetrakis[4-sulfonatophenyl]porphyrin) (Chart 1) against PC/CL (phosphatidylcholine/cardiolipin, 85/15%) liposomes as a model of the lipid fraction of the inner mitochondrial membrane. The lipid damage was analyzed by peroxide dosage, conjugated dienes, thiobarbituric reactive substances (TBARs) and giant unilamellar vesicles (GUVs) images from optical microscopy and DCF fluorescence. The use of GUVs allows a real-time visualization of the oxidative damages in a membrane model. A mimetic model of the inner mitochondrial membrane was chosen, because the cationic porphyrin TMPyP has been described to accumulate in mitochondria (22,23).

MATERIALS AND METHODS

Chemicals. TMPyP (*meso*-tetrakis [*N*-methyl-4-pyridyl]porphyrin), TPPS4 (*meso*-tetrakis[4-sulfonatophenyl]porphyrin), 2′,7′-dichlorodihydrofluorescein diacetate (H_2DCF-DA), sorbic acid, sodium azide, phosphoric acid, thiobarbituric acid (TBA) and percloric acid ($HClO_4$) were purchased from Sigma-Aldrich Corp. (St. Louis, MO, USA). Xylenol orange was purchased from Fluka Chemical Corp. (Ronkonkoma, NY, EUA). Glucose, sucrose, ammoniacal ferrous sulfate ($[NH_4]_2Fe[SO_4]_2$), chloroform, *n*-buthanol and ethanol were obtained from Synth (Labsynth Ltda., SP, Brazil). L-α-phosphatidylcholine from egg (PC), cardiolipin bovine heart (CL), dipalmitoyl phosphatidylcholine (DPPC), dioleoyl phosphatidylcholine (DOPC) and tetraoleoyl cardiolipin (TOCL) were purchased from Avanti Polar Lipids (Alabaster, AL, USA). Deuterium oxide (D_2O) was purchased from Cambridge Isotope Laboratories, Inc. (Andover, MA, EUA). The TMPyP stock solution concentration was checked using the absorption coefficient $\varepsilon_{423nm} = 2.26 \times 10^5$ M^{-1} cm^{-1} and TPPS4 at $\varepsilon_{412} = 5.30 \times 10^5$ M^{-1} cm^{-1} (37).

Generation of photo-oxidative species. Where indicated, porphyrins were excited by irradiation with a white LED array. The LED array emits 200 μW/cm^2 in 532 nm measured by FieldMate powermeter (Coherent Inc.). The laser presented a 10 mW power measured by the same powermeter.

Lipid oxidation assays:. Lipid oxidation was evaluated with lipid peroxide (LOOH) and TBARS production. Lipid hydroperoxide concentration was determined by the oxidation of Fe(II) in the presence of xylenol orange: aliquots of the sample (10 μL) were extracted from incubation at room temperature and mixed with 890 μL of Milli-Q® water and 100 μL of hydroperoxide reagent that contained 2.5 mM xylenol orange, 2.5 mM $(NH_4)2Fe(SO_4)_2$ and 1.15 M $HClO_4$ in Milli-Q® water. The mixture was incubated for 30 min at room temperature. The oxidation of Fe(II) by LOOH generates Fe(III), which reacts with xylenol orange and is converted to the colored product that absorbs at 560 nm. LOOH concentration was calculated by using $\varepsilon = 560$ nm $= 6.45 \times 10^4$ M^{-1} cm^{-1}. TBARS was determined at 535 nm after reaction with TBA, using the molar extinction coefficient 1.56×10^5 M^{-1} cm^{-1}.

Electronic absorption spectra measurements. The electronic absorption spectra of porphyrins were measured by using a Varian Cary 50, Varian Inc. (CA, United States) spectrometer. The spectral resolution for wavelength scan was 0.5 nm. The optical path length was 1 cm for the LOOH, TBAR and DCFH dosages, and 0.1 cm for the porphyrin spectra measurements.

Giant unilamellar vesicles (GUVs). Giant unilamellar vesicles of PC/CL (80/15 mol%, respectively) were grown using the electroformation method (38,39). Briefly, 40 μL of a mixture of lipids 2.5 mM in chloroform solution was spread on the surfaces of two conductive glass plates (coated with indium tin oxide). The apparatus were positioned with the conductive sides facing each other and separated by a 2-mm-thick Teflon frame. In the following, the electroswelling chamber was filled with a 0.2 M sucrose solution, and connected to an alternating power generator at 1 V with a 10 Hz frequency for 2 h at 25°C. The vesicle suspension was removed from the chamber and diluted ~6 times into 0.2 M glucose solution. In this condition, spherical GUVs were obtained with diameters in the range of 10 μm. The sugar optical asymmetry between the interior and the exterior of the vesicles created differences in density and in the refractive index between the sucrose and glucose solutions; the vesicles were, therefore, stabilized by gravity at the bottom of the chamber, and had the best contrast when observed under phase contrast microscopy. The observation of giant vesicles was performed by phase-contrast microscopy.

Optical trap and phase-contrast microscopy images. Home-made optical tweezers were employed to trap and to image isolate GUVs (Magrini, T. and Martinho, H., unpublished results). The optical tweezer was composed by a 975 nm Pigtailed Laser Diode (Butterfly Package PL980P330J), a set of lenses, mirrors and a Nikon 100× Oil Immersion Objective for collimating laser light. The laser power was less than 5 mW in the trapped GUV. ACCD USB DCU224C camera with a resolution of 1280 × 1024 pixels and a field of 70× 87.6 μm was used to capture the images. The public domain software Image J (Wayne Rashand, rsb.info.nih.gov/ij/) was used to process and analyze the captured images. The radial intensity distribution profile as function of time was used to obtain quantitative pieces of information concerning the structural variations.

Generation of DCF by the photodynamic action of photosensitized porphyrins. DCFH (Sigma) was obtained by hydrolysis of its diacetate

form (H_2DCF-DA, 2′, 7′-dichlorodihydrofluorescein diacetate). Briefly, an appropriate aliquot from a H_2DCF-DA stock solution (200 μM) was added to an aliquot of NaOH (50 mM) in the dark, kept on ice for 30 min in the dark, and used in the same day of its preparation. The solution of the hydrolyzed product was then neutralized with an appropriate volume of hydrochloric acid to a pH of 7.2. DCF, which is the fluorescent product of DCFH oxidation, emits at λ_{max} = 522 nm when excited at 490 nm (40–42). Fluorescence spectra were obtained with a Varian Cary Eclipse fluorimeter, Varian Inc. (CA, USA). All measurements were made just after each irradiation procedure and at room temperature. The time dependence of DCF fluorescence was fitted to,

$$F(t) = F_{max} \times (1 - e^{-t*k}) \quad (1)$$

by using Origin (Microcal) software. F_{max} is the asymptotic of the rate curve, and k is the observed rate constant.

Determination of zeta potential (ζ). The measurements were carried out in a Zetasizer Nano ZS, Malvern Instruments, Ltd. (London, UK), at the temperature of 25°C. The ζ is determined by the electrophoretic mobility, μ_e by the application of the Henry equation and calculated by using the Smoluchowski approximation. The ζ values are the average of 10 independent measurements that were calculated using a mono-modal model and time measurement was determined by the instrument. For each zeta potential measurements, the samples were previously equilibrated for 1 min at 25°C.

RESULTS AND DISCUSSION

Interactions of TMPyP and TPPS4 with PC/CL liposomes

The electronic absorption spectra of TMPyP and TPPS4 are typical of porphyrins with D2h molecular symmetry (Fig. 1). TMPyP (black line) and TPPS4 (gray line) exhibit, respectively, the intense Soret bands at 423 and 410 nm and the following lower intensity Q bands: Q_y(0,0) at 518 and 516 nm, Q_y(0,1) at 555 and 553 nm, Q_x(0,0) at 586 and 584 nm and Q_x(1,0) at 644 and 634 nm (17,43–46). Figure 1 (right scale) shows that the emission spectrum of the white LED used for the electronic excitation of the porphyrins overlaps their Q bands.

The electronic absorption spectrum of TMPyP presented significant changes in the presence of PC/CL liposomes. The interaction between the cationic free base TMPyP and the negatively charged PC/CL liposomes changed the energy of π–π* transitions, leading to red shifts in the Soret and Q bands. The Soret band shifted 5 nm and peaked at 428 nm. The peaks of Q bands Q_y(0,0), Q_y(0,1), Q_x(0,0) and Q_x(1,0) shifted to 521, 557, 592 and 648 nm, respectively. The left and right panels of Fig. 2A show, respectively, the spectra of TMPyP and TPPS4 in a homogeneous medium (gray lines) and in the presence of PC/CL liposomes (dashed lines). The turbidity promoted by the presence of liposomes was subtracted from the original data, and the resulting spectra of the porphyrins presented as black lines. Figure 2A (right panel) shows the spectra of TPPS4 in the presence of 1 mmol L^{-1} of PC/CL liposomes. The presence of PC/CL liposomes did not promote significant spectral changes in the anionic porphyrin, indicating the low affinity of TPPS4 for the negatively charged lipid interface.

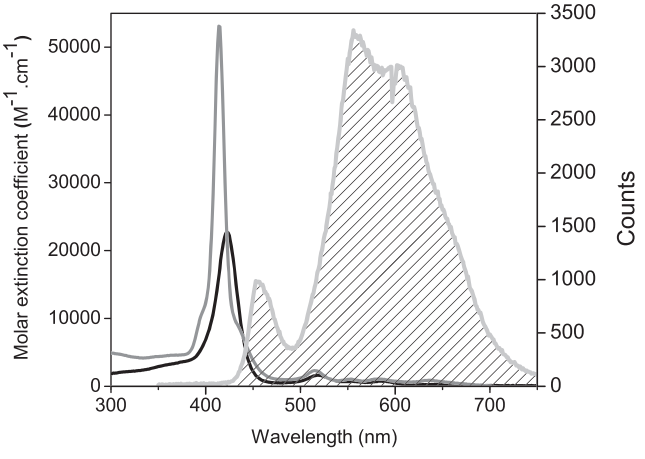

Figure 1. Overlapped electronic absorption spectra of the porphyrins TMPyP and TPPS4 on the emission spectra of the lamps used for electronic excitation of the photosensitizers. The spectrum of TMPyP in 0.2 M glucose is shown as a black line, and the TPPS4 spectrum is shown as a gray line. The emission spectrum of the white LED light source is the gray area.

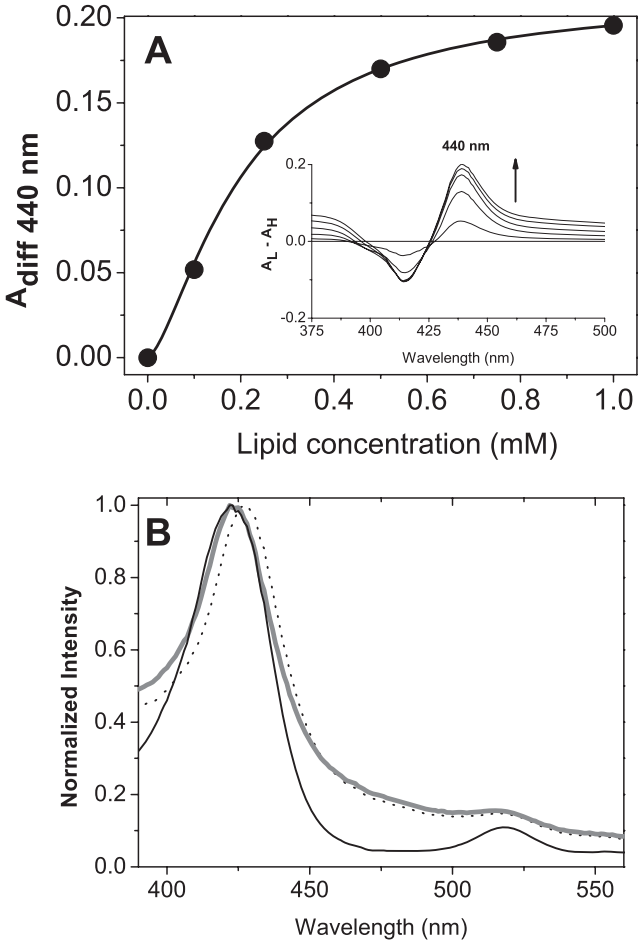

Figure 2. Effect of PC/CL liposomes on the electronic absorption spectra of TMPyP and TPPS4. (A) Intensity of the differential TMPyP Soret band at 440 nm plotted as a function of lipid concentration. The data were obtained from the differential spectra of TMPyP at increasing lipid concentrations (0.1, 0.25, 0.5, 0.75 and 1.0 mM PC/CL, respectively), as indicated by the arrow in the inset. (B) Normalized electronic absorption spectra of TMPyP in different media. The spectrum of TMPyP in 0.2 M of glucose is shown as a black solid line, the spectrum of TMPyP in the presence of 1 mM PC/CL (85/15 mol %) liposomes as a dotted line and the spectrum of TMPyP dissociated from the negatively charged interface by addition of 300 mM of NaCl as a gray line.

The porphyrin/lipid interaction was better evaluated by the analysis of the differential spectra obtained from the subtraction of the porphyrin spectrum in aqueous homogeneous media from those obtained in the presence of different lipid concentrations. Figure 2A shows the intensity of Soret band differential spectra at 440 nm plotted as a function of lipid concentration. The differential spectra are shown in the inset of Fig. 2A. The data were best fitted by Eq. (2) derived from the binding equilibrium (47,48):

$$A_L - A_0 = \frac{nk_b[L]_T}{1 + k_b[L]_T} \quad (2)$$

where $A_L - A_0$ is the differential absorbance intensity at different lipid concentrations and k_b is the binding constant. The fitting according to Eq. (1) resulted in k_b = 9, 2 (±) 10^3 M^{-1}.

TMPyP is a hydrophilic porphyrin, and it is not expected to be found buried in the bilayer. Thus, these spectral changes can be assigned to an electrostatic interaction of the positively charged metal-free TMPyP *meso* ligands with the negatively charged interface of PC/CL (32,49).

The binding of TMPyP on PC/CL liposomes was also corroborated by zeta potential measurements. The zeta potential measured for PC/CL liposomes in the presence and in the absence of TMPyP presented results similar to that previously presented by Neto *et al.*, 2013 (34). The authors studied the binding of TMPyP on POPC:POPG LUVs with different percentages of the anionic phospholipid (PG). The zeta potential (ζ) of PC/CL (85% PC and 15% CL) in the absence and in the presence of 10 μM TMPyP was −42.5 and −39.5 mV, respectively. These results are consistent with the occurrence of electrostatic interaction between the negatively charged phospholipid and the cationic *meso* ligands of TMPyP.

The electrostatic interaction mechanism that binds TMPyP to PC/CL liposomes was further reinforced by the addition of NaCl in a medium containing TMPyP associated with liposomes (Fig. 2B). The increase in ionic strength reversed the spectral change in TMPyP promoted by PC/CL liposomes.

Photodynamic effects of TMPyP and TPPS4 on PC/CL large unilamellar vesicles (LUVs)

To model the effects of PDT on the lipid fraction of biological membranes, TMPyP and TPPS4 were used for the photo-oxidation of phospholipids, PC and CL, arranged as LUVs (Fig. 3A and B). Figure 3A shows the spectral changes in the porphyrin-containing PC/CL liposomes in the course of the irradiation with white LED (spectrum shown in Fig. 1). In the presence of TMPyP (left panel), the partial bleaching of the porphyrin concomitant with an increase in the absorbance at 234 nm ($\Delta A_{234\ nm}$ around 0.2) was observed after 60 min of irradiation.

The increase in absorbance of lipids at 234 nm is suggestive of the formation of conjugated dienes (50). In the presence of TPPS4 (right panel), the increase in absorbance in the 234 nm region during 60 min of irradiation was not significant ($\Delta A_{234\ nm}$ around 0.02). Furthermore, the lipid oxidation was not associated with significant porphyrin bleaching (Fig. 3A, right panel). The lower panel of Fig. 3B shows that the LOOH content of the PC/CL vesicles increased significantly over the course of a 60-min irradiation in the presence of TMPyP and TPPS4 when the vesicles were under conditions that are identical to those described above. However, the cationic TMPyP was more efficient than the anionic TPPS4 was at damaging the phospholipids. After 60 min of irradiation in the presence of TPPS4, the LOOH content of the PC/CL vesicles increased more than two-fold, that is from 2 to 5.5 μM. In the presence of TMPyP, the production of LOOH was higher and faster. The LOOH content in the presence of TMPyP increased almost eight-fold relative to the control after 15 min of irradiation using the white LED. Lipid oxidation was not observed when the vesicles were incubated during 60 min with the porphyrins in the dark (Fig. 3B, black columns in the upper panel). Similar results were obtained by using the green laser to promote the electronic excitation of TMPyP (not shown).

Photodynamic effects of TMPyP and TPPS4 on PC/CL giant unilamellar vesicles (GUVs)

The photodynamic effects of TMPyP and TPPS4 were also probed in the presence of PC/CL GUVs. Figures 4A and B show contrast phase images of GUVs during irradiation in the presence of TMPyP and TPPS4, respectively. These images were extracted at the indicated times from the movies recorded during the irradiation of GUVs in the presence of porphyrins. The edited movies are available in the supplementary material section. We notice that GUVs in the dark were not damaged by the porphyrins, and remained stable for hours (not shown). However, when maintained under irradiation with the white LED, the GUVs underwent significant alterations. Figure 4A shows images consistent with progressive damage of a PC/CL GUV during almost 18 min of irradiation in the presence of TMPyP. The image obtained at 10 min of irradiation in the presence of TMPyP shows that the GUV became leaky. The leakiness of GUV initiated at ~7 min as evidenced by Fig. 4C showed bellow. The crescent contrast loss on the vesicle that culminates with vesicle disruption at around 15 min attests to the leakiness of the GUV. In the presence of TPPS4, the irradiation of GUVs led also to damage in the membrane with a peculiar behavior. In the course of the irradiation, undulations were apparent; therefore, the GUV undulated and produced encapsulated daughter vesicles (internal buds) (Fig. 4B).

The formation of daughter vesicles in GUVs has been described for GUVs that contain raft mixtures and were submitted to osmotic stress (51). After 34 min of irradiation, the GUV encapsulating the smaller sized GUVs expelled the internal smaller vesicles that are apparently connected and resemble a tail linked to the mother GUV (see the zoom of the smaller GUVs detected at 39′27″ of irradiation). After the exclusion of most of the small daughter GUVs, the mother vesicle was significantly smaller (around 1/4 of its initial size) but without significant loss of contrast. At the ultimate irradiation times, the process also culminated in vesicle disruption. Figures 4A and B are representative of a set of different independent experiments.

To obtain a quantitative view of the loss of contrast, each image was converted to a radial intensity distribution plot, as shown in the upper and lower panels of Fig. 4C. The leakage of GUV shares internal and external bulk solution, and abolishes the difference in the refraction index, leading to loss of image contrast. The upper panels of Fig. 4C show the normalized intensity at the radial coordinates of a selected GUV image at the initial (black line) and final (gray line) time of irradiation in the presence of TPPS4 (left upper panel) and TMPyP (right upper panel). The minimum and maximum of the plot

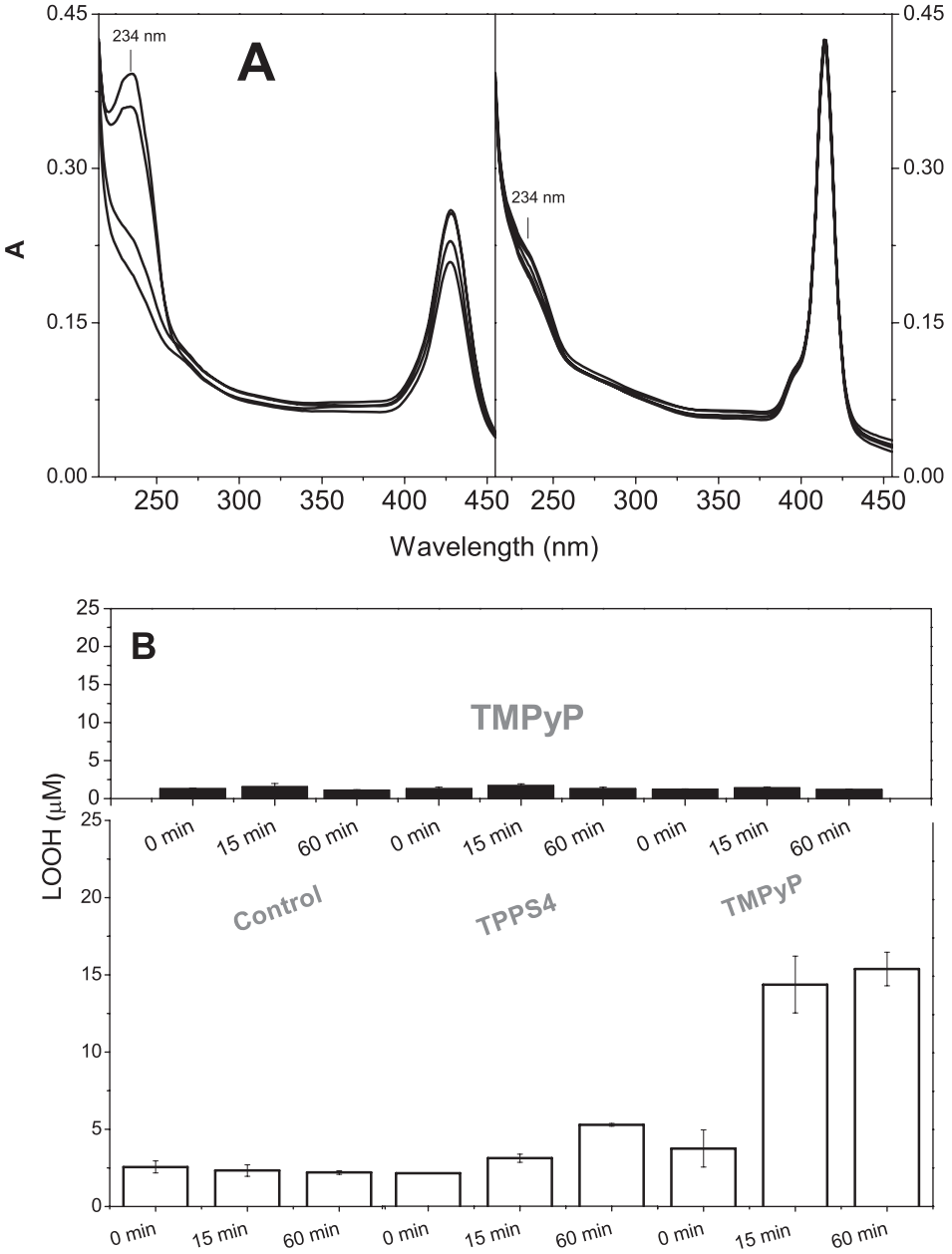

Figure 3. Photodynamic effect of TMPyP and TPPS4 on PC/CL liposomes. (A) Effect of white LED irradiation on the electronic absorption spectra of 10 μM of TMPyP and TPPS4 in the presence of PC/CL liposomes. The spectra were recorded at 0, 15 and 60 min of irradiation. (B) Lipid photo-oxidation promoted by 10 μM of TPPS4 and TMPyP. The lower panel shows time-dependent formation of LOOH in the absence (control) and in the presence of the porphyrins as indicated over the corresponding results. The upper panel shows the results obtained in the same above-mentioned conditions except that the samples were incubated in the dark. Experiments were carried out using PC 85% and CL 15% 1 mM in a medium of 0.2 M of glucose.

correspond to the darker and brighter portion of the GUV image, respectively. The corresponding radii were labeled r_{int} and r_{ext}. Insets in the right and left upper panels of Fig. 4C show representative contrast phase images of optically trapped GUVs during irradiation in the presence of TMPyP and TPPS4, respectively. One could measure the loss of contrast by measuring the visible thickness of the GUV membrane. This thickness could be estimated by finding the difference between r_{ext} and r_{int}. The values of $r_{ext}-r_{int}$ as a function of time are shown in the bottom panels of Fig. 4C. These plots are consistent with the loss of contrast phase that occurs only in the presence of TMPyP**.**

In a speculative way different results obtained for GUVs challenged by the photodynamic action of TPPS4 and TMPyP might result from the topology of the porphyrins with repercussions on the site of singlet oxygen generation. TPPS4 and TMPyP were added in the suspension of GUVs and it is not expect that the hydrophilic photosensitizers can attain the internal compartment of these vesicles. TPPS4 in the external bulk phase generated singlet oxygen in the same location. Therefore, this excited species diffused and accessed GUVs by the external face probably having the lipids in the external leaflet as the preferential target. The putative asymmetrical oxidative damage might be enough to create a surface tension that resulted in buds, formation and

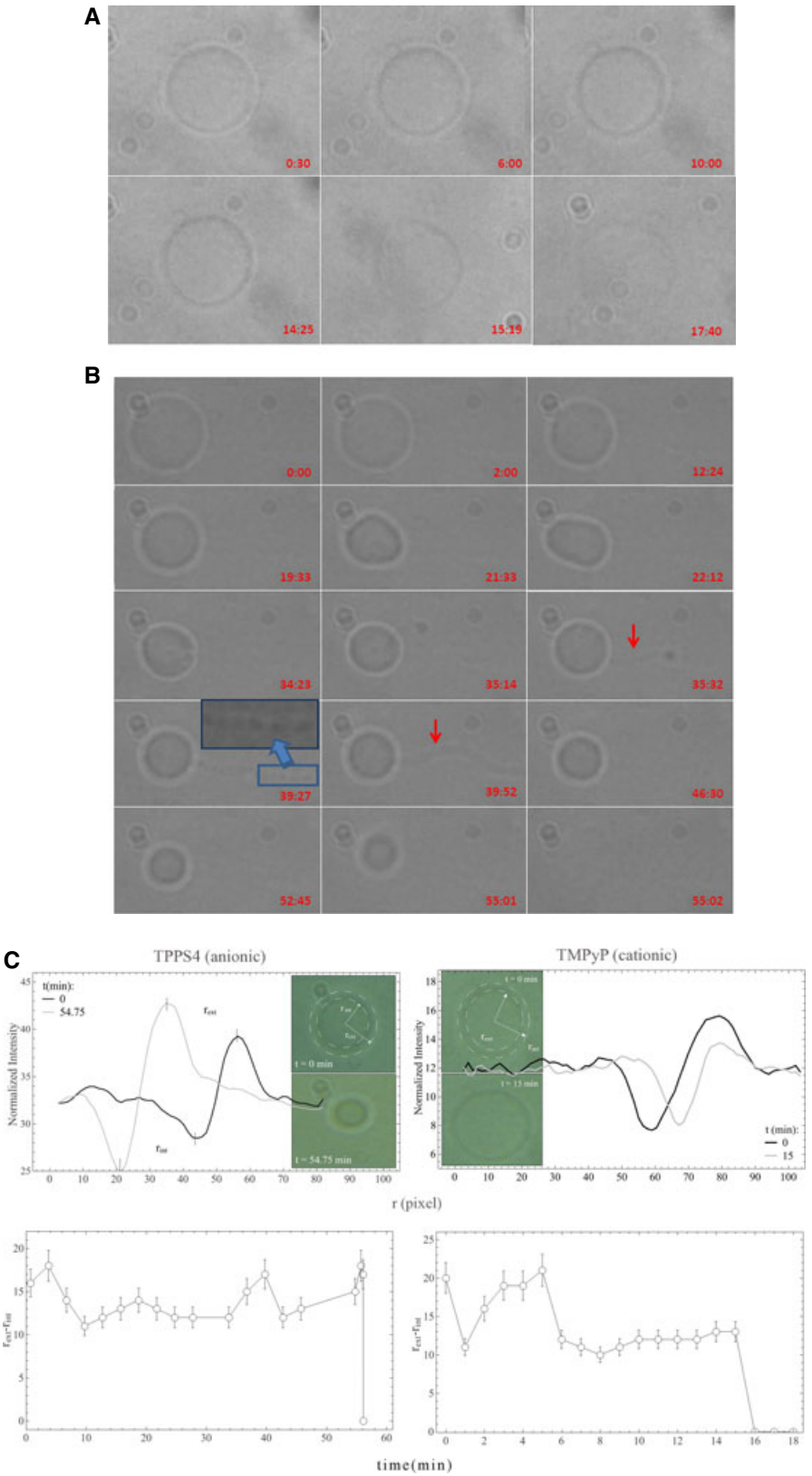

Figure 4. Effect of porphyrins on PC/CL Giant Unilamellar Vesicles (GUVs). (A) Phase contrast microscopy images of optically trapped PC/CL GUV in the course of irradiation in the presence of TMPyP. (B) Phase contrast microscopy images of optically trapped PC/CL GUV during irradiation in the presence of TPPS4. (C) Decrease in the area of the PC/CL GUV contrast phase image during irradiation in the presence of TPPS4. The PC/CL (85/15 mol%) GUV was prepared in 0.2 M sucrose, and the vesicle suspension was six-fold diluted in 0.2 M of glucose.

expulsion of small daughter vesicles. These events are responsible for the significant decrease in GUV radius. Differently, TMPyP localized at GUV external interface generated singlet oxygen dissolved in the lipid bilayer that might promote a symmetrical oxidative damage at the two lipid leaflets. In this case, the putative symmetrical oxidative event promoted relative rapid vesicle leak resulting in the observed loss of contrast without significant changes in vesicle radius.

Mechanism of photodamage of PC/CL liposomes promoted by porphyrins

The photoproduction of LOOH observed during the irradiation of PC/CL vesicles in the presence of the porphyrins was not accompanied by a significant increase in TBARS (not shown). This result suggests that the Type-II mechanism, that is the addition of $O_2(^1\Delta_g)$ to a double bond of a polyunsaturated fatty acid (PUFA), was the principal contributor to the conjugated dienes and LOOH production. Singlet oxygen reacts with olefins owing a structure with two or more allylic substituents. This reaction promotes a double bond shift concomitant with the formation of an allylic hydroperoxide (52–54). Therefore, in the Type-II mechanism, $O_2(^1\Delta_g)$ adds to a lipid double bond and converts LH to LOOH without the formation of a peroxyl radical intermediate. In the Type-I mechanism, a peroxyl radical can be converted to TBARS after subsequent reactions (Scheme 1). Detailed discussions about the singlet–oxygen-mediated lipid peroxidation mechanisms can be found in references (55–57).

To investigate the predominant mechanism responsible for lipid peroxidation, PC/CL liposomes were exposed to the photodynamic action of TMPyP and TPPS4 in the presence of D_2O and in the presence of quenchers of the excited states generated in the medium during photosensitization of the porphyrins (Fig. 5A and B). Figure 5A shows that the LOOH content of PC/CL liposomes, which is produced after 60 min irradiating TPPS4 in D_2O (light gray column in central panel), was twice and a half higher than that produced in aqueous medium (diagonal striped column in central panel). When TMPyP was used as the sensitizer, the LOOH content (light gray column in right panel of Fig. 5A) that was produced in D_2O was circa 37% higher than that produced in an aqueous medium (diagonal striped column in right panel of Fig. 5A). D_2O had no effect on the LOOH content of the system in which porphyrins are absent (control). These results are consistent with the contribution of $O_2(^1\Delta_g)$ for the generation of LOOH by both the photosensitized TMPyP and TPPS4. The differences in the increase in LOOH production promoted by D_2O could be assigned to the different microenvironments in which the excited species are produced (see below).

Figure 5B shows that sorbic acid (yellow column) and sodium azide (light red column) were able to promote significant decrease in the LOOH produced by TMPyP in D_2O. This result is also consistent with the contribution of $O_2(^1\Delta_g)$ for the production LOOH by TMPyP. Sorbic acid quenches triplet TMPyP and prevents the energy transfer to molecular oxygen. On the other hand, sodium azide quenches $O_2(^1\Delta_g)$ produced by energy transfer from triplet TMPyP. The inhibitory effect of sodium azide on the lipid peroxidation promoted by TMPyP provided an additional support for the contribution of a Type-II mechanism in the lipid peroxidation. Sorbic acid (around 70% inhibition) was more efficient than sodium azide (around 50% inhibition) at inhibiting lipid peroxidation by the photodynamic action of TMPyP. A probable cause can be found in the topology of the porphyrin in the membrane and at the site of $O_2(^1\Delta_g)$ production. TMPyP should be associated on the membrane surface and probably transfers most of the electronic excitation energy to the molecular oxygen inside the bilayer.

Thus, sodium azide can quench $O_2(^1\Delta_g)$ molecules moving to (or formed in) the bulk; however, it has limited access to the $O_2(^1\Delta_g)$ that remains inside the bilayer. In the presence of sorbic acid and azide, saturation of the damage was attained at 15 min of irradiation, and at which point, it was used the 15 min irradiation time. Meanwhile, in the absence of quenchers, an increase in LOOH was observed at 60 min. The above-mentioned results are in agreement with the recent study by Ehrenberg *et al.*, 2013 (58). The authors state that singlet oxygen quenching by azide depends on a physical encounter with this excited species during its short lifetime. They demonstrated that in the presence of positively charged liposomes azide is concentrated in the Debye layer near the surface of the bilayer. Otherwise, azide is preferentially in the bulk solution when negatively charged liposomes are present. PC/CL liposomes are negatively charged and in this condition azide can efficiently quencher singlet oxygen that is generated in the bulk phase. Equally, in this study, the heterogeneous medium is responsible for the differentiated effects of D_2O observed for TPPS4 and TMPyP. In the presence of liposomes, increase in singlet oxygen lifetime by D_2O can be observed only for the excited species diffusing in the bulk phase. Therefore, the minimal lipid photooxidation enhancement in D_2O compared to H_2O that was observed for TMPyP is consistent with the proposal that the cationic porphyrin binds to the anionic surface of PC/CL liposomes and generates singlet oxygen inside the lipid bilayer.

Considering that $O_2(^1\Delta_g)$ adds to a double bond of a PUFA leading to LOOH production, lipid peroxide derivatives are expected to be produced in phospholipids in which the glycerol moiety is exclusively esterified with oleic acid. Figure 6 shows that the LOOH content of DOPC/TOCL vesicles submitted to the photodynamic action of TMPyP increased five-fold after 60 min of irradiation.

Although the production of LOOH had been four-fold lower when biological PUFA-containing phospholipids had been replaced by oleoyl-containing phospholipids, this result is also consistent with $O_2(^1\Delta_g)$ as the prooxidant agent for LOOH production. The lower yield of LOOH in the presence of DOPC/TOCL could be assigned principally to TOCL (15% of the lipid content) as the preferential target for $O_2(^1\Delta_g)$. The cationic porphyrin is expected to bind preferentially on CL domains. Therefore, when PUFA-containing CL is present in the liposome, a higher amount of double bonds are available for the $O_2(^1\Delta_g)$ attack, and the production of LOOH is higher.

Contributions of topology and quantum yield of TMPyP and TPPS4 to membrane damage

Although different results obtained with TMPyP and TPPS4 have been consistent with the different topologies of the cationic and anionic porphyrins in an aqueous medium containing negatively charged vesicles, it is important to consider the photochemical behavior of the investigated porphyrins *per se*. Thus, oxidative conversion of DCFH into DCF, that is the fluorescent species (Scheme 2), by the photodynamic action of TMPyP and TPPS4

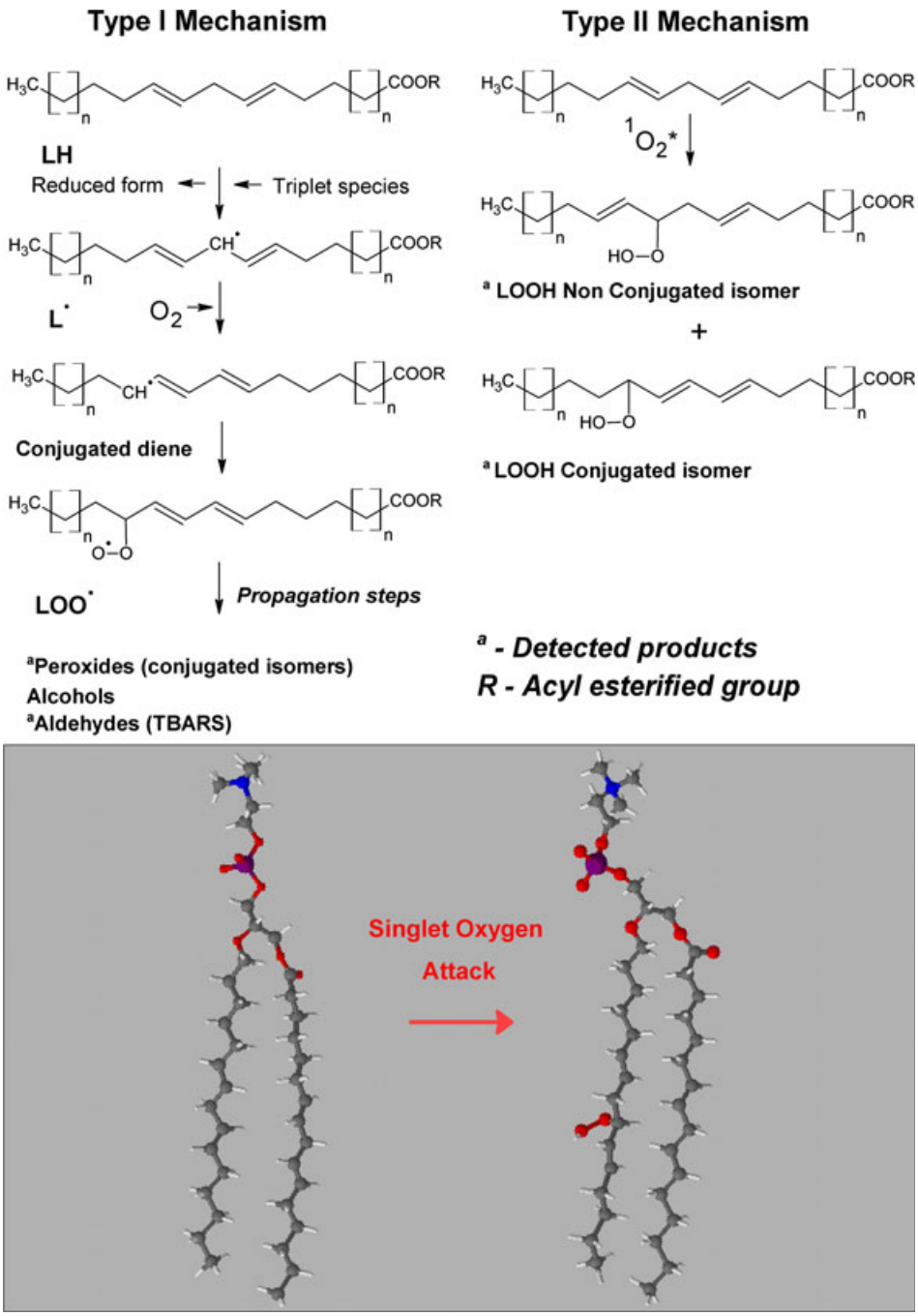

Scheme 1. Mechanisms of LOOH production by free radicals and $O_2(^1\Delta_g)$. In Type I and II mechanisms, respectively, molecular oxygen and singlet molecular oxygen also react on the right hand portion since the compound is unsymmetrical. The gray box shows a cartoon with the 3D structure of a phospholipid and the peroxide-derivative form after singlet oxygen attack.

was investigated in the absence and in the presence of PC/CL liposomes (Fig 7).

Peculiar results were obtained by comparing the action of TMPyP and TPPS4 on DCFH under different conditions. The yield of DCF produced by the oxidation of DCFH in a homogeneous medium after 25 min of irradiation in the presence of TMPyP was five-fold lower than that obtained when TPPS4 was the photosensitizer. Contrary results, that is the yield of DCF generation being five-fold higher for TMPyP, were obtained in the presence of DPPC/TOCL liposomes. The partition coefficient for DCFH is 2.62 (59), so this fluorescent probe can scavenge pro-oxidant species within lipid bilayers as well as in the aqueous phase. Therefore, this result is consistent again with the presence of TMPyP at the liposome interface and TPPS4 partitioned preferentially in the bulk (upper panels of Fig. 7). At the interface of DOPC/TOCL, TMPyP can generate $O_2(^1\Delta_g)$ at the bulk interface and in the bilayer. Binding of sensitizers on the membrane surface can enhance the pro-oxidant effectiveness on membrane components and partitioned molecules due to three principal reasons: (1) the higher concentrations of oxygen in

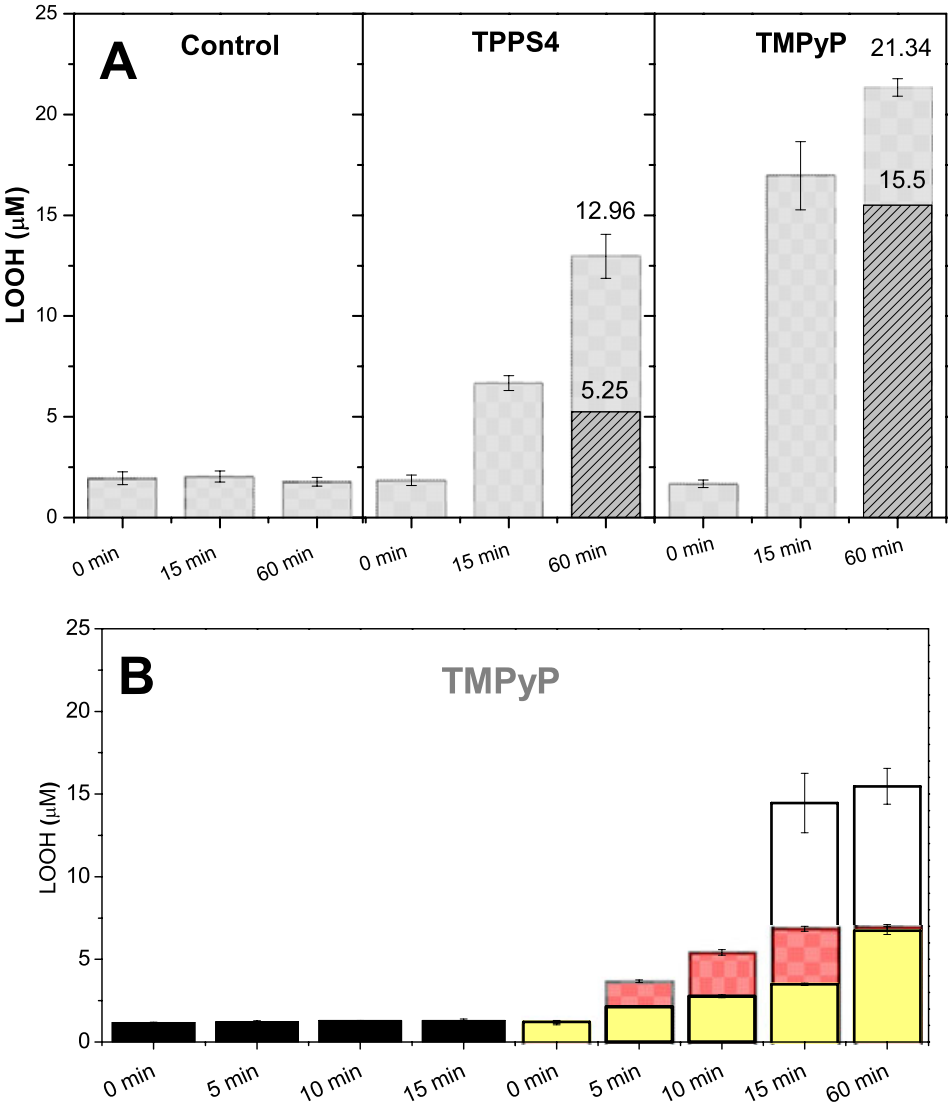

Figure 5. Effect of modifiers of the lifetime of the excited species on lipid photo-oxidation promoted by porphyrins**.** (A) Effect of deutered water (D_2O) on lipid photo-oxidation promoted by TPPS4 and TMPyP. Experiments were carried out using 1 mM PC/CL liposomes in medium D_2O (light gray bars) containing 0.2 M of glucose in the absence (control) or in the presence of 10 μM of TMPyP and TPPS4 as indicated over the gray columns. The overlapped columns filled with a diagonal stripe pattern correspond to the results obtained in the same conditions except that D_2O was replaced by H_2O. (B) Effect of triplet species quencher (1 mM of sorbic acid, presented as ■ columns) and $O_2(^1\Delta_g)$ quencher (1 mM sodium azide, presented as ■ columns) on the lipid photodamage promoted by 10 μM of TMPyP. The white and black columns represent the results obtained in the absence of quenchers for the samples incubated under irradiation and in the dark, respectively. The samples were irradiated using white LED.

lipid membranes that are estimated to be around one order of magnitude greater than in the bulk aqueous media; (2) the longer photosensitizer triplet-state and $O_2(^1\Delta_g)$ lifetimes in membranes relative to aqueous solution (60–64) (3) and the confinement of $O_2(^1\Delta_g)$ at smaller distances of the target molecules. In fact, there is a correlation between the efficiency of sensitizers and their affinity for lipid bilayers (60,65). It is important to consider that the stability of the photosensitizer also influences the total amount of DCFH that is converted to DCF. Consistently, in a homogeneous medium, TMPyP exhibited significant bleaching whereas TPPS4 remained unchanged (not shown). Conversely, the presence of PC/CL liposomes increased the stability of TMPyP. Therefore, two factors contributed to the higher production of DCF by TMPyP in liposomes: the stability of the sensitizer and its association with the lipid bilayer where a higher concentration of molecular oxygen is present.

However, the lower panels of Fig. 7 show that in the homogeneous medium as well as in PC/CL liposomes, TMPyP converted DCFH to DCF three-fold and a half faster than did TPPS4 ($4.8 \pm 0.1 \times 10^{-3}$ s^{-1} *versus* $1.4 \pm 0.1 \times 10^{-3}$ s^{-1}) in the homogeneous medium and four-fold and a half faster than TPPS4 ($2.3 \pm 0.7 \times 10^{-3}$ s^{-1} *versus* $0.5 \pm 0.1 \times 10^{-3}$ s^{-1}) in DPPC/TOCL liposomes. Relative to TPPS4, the relatively higher rate of DCF photogeneration by TMPyP (both in homogeneous and heterogeneous media) could be related to the quantum yield of $O_2(^1\Delta_g)$ (Φ_Δ) generated by energy transfer from the triplet state of the cationic porphyrin. The Φ_Δ values for TMPyP reported in literature are somewhat controversial, varying from 0.58 (66) to 0.9 (67). However, the latter value seems to be overestimated, and the more plausible value is 0.74 (68), whereas the Φ_Δ of deprotonated TPPS4 has been reported to be 0.62 ± 0.03 (66).

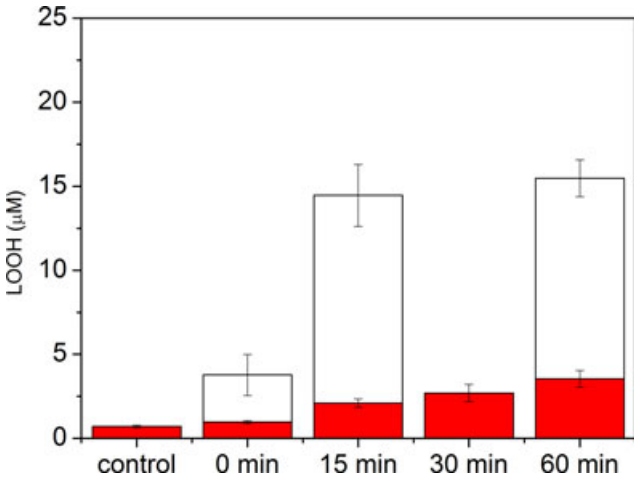

Figure 6. Effect of the lipid composition on the production of LOOH by the photodynamic action of TMPyP. The columns represent the LOOH production after the irradiation of PUFA-containing PC/CL, and the ■ columns represent the LOOH production after the irradiation of DOPC/TOCL.

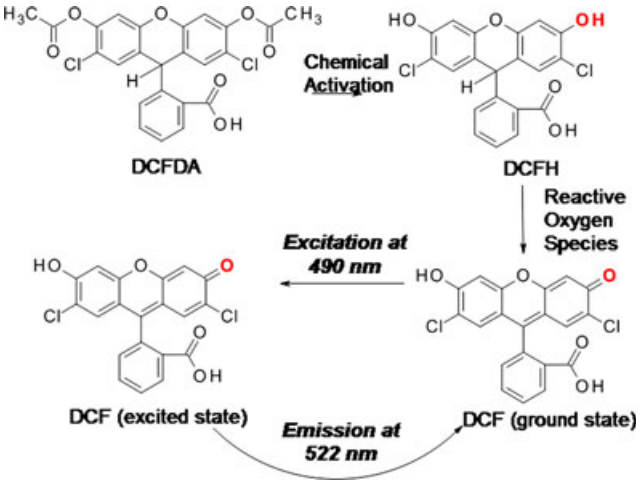

Scheme 2. Detection of pro-oxidant species by DCFH.

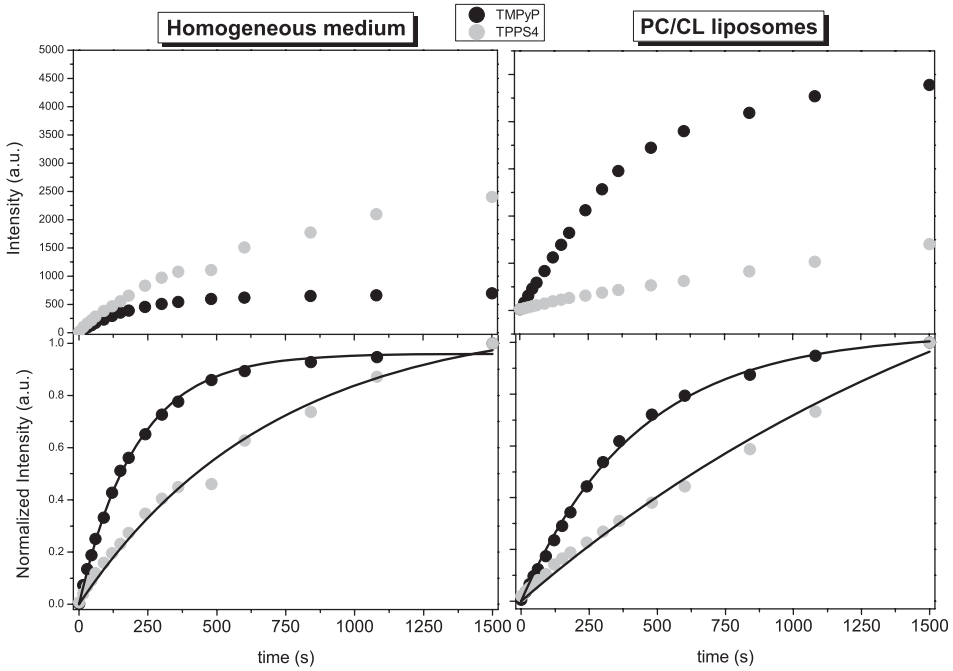

Figure 7. Photo-oxidative production of DCF by TMPyP and TPPS4. Upper panels show the increase in fluorescence during the irradiation of TMPyP (black circles) and TPPS4 (light gray circles) in homogeneous media (left) and in PC/CL liposomes (right). The lower panels show the normalized data fitted by Eq. (1). Experiments were carried out using 0.5 μM of DCFH in the presence of 5 μM of porphyrins in an aqueous medium containing 0.2 M of glucose (left) or in the presence of PC/CL liposomes (right). The samples were irradiated with white light LED for 1500 s, and the fluorescence was measured at the indicated times. The fluorescence λ_{max} at 522 nm was measured at room temperature by excitation at 490 nm using slits of 5/5 nm.

Thus, it is evident that affinity to the biological target is important for the photodamage degree in PDT. On the other hand, the capacity of singlet oxygen to diffuse and to attain distant target molecules permits a photosensitizer with low affinity to a biological structure to cause photodamage via the Type-II mechanism. An example of the long-range effect of the Type-II mechanism was provided by undulations, involutions and disruption of PC/CL GUVs submitted to the photodynamic action of TPPS4.

CONCLUSION

This report presents the study of the effects of the PDT on a model of the inner mitochondrial membrane under two conditions: using a photosensitizer without affinity to the membrane (anionic porphyrin) and a photosensitizer that binds to the membrane by means of electrostatic interactions (cationic porphyrin). As expected, only TMPyP binds electrostatically to PC/CL liposomes; however, both porphyrins were able to damage

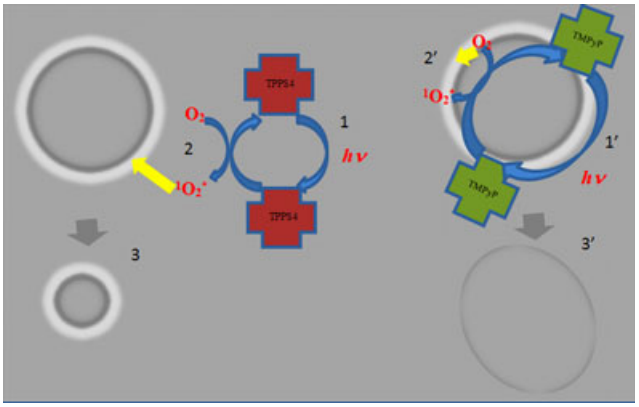

Scheme 3. Photodynamic effects of TPPS4 and TMPyP modulated by the topology of the sensitizers. In the left side, TPPS4 is in the bulk water and after electronic excitation (1) decays via energy transfer to molecular oxygen dissolved in bulk water generating singlet oxygen (2). Singlet oxygen travels to the membrane of a GUV and promotes oxidative damage (yellow arrow). After ~50 min GUV was significantly smaller but without significant loss of contrast. TMPyP bound to GUV membrane, after electronic excitation (1′) decays via energy transfer to molecular oxygen dissolved into the lipid bilayer generating lipid dissolved singlet oxygen. Singlet oxygen dissolved in lipid bilayer (2′) attacks lipid acyl chains (yellow arrow). After ~15 min, GUV exhibited was leaky evidenced by loss of contrast (3′).

the membrane via the Type-II mechanism. Taken together, the results obtained in the presence of D_2O, quenchers of the excited species and by using DCFH as a probe of pro-oxidant species suggest that the binding to PC/CL lipid bilayers had two principal effects on the photodynamic action of TMPyP: (1) the increase in TMPyP stability, leading to a higher production of lipid and DCF photoproducts, and (2) the generation of long-lived $O_2(^1\Delta_g)$ by the sensitization of molecular oxygen partitioned in the lipid bilayer. Regarding the quantum yield of $O_2(^1\Delta_g)$ production, TPPS4 and TMPyP exhibit close values (0.62 and 0.74, respectively) (67,68) in aqueous media, but TMPyP is more susceptible to photobleaching than TPPS4. Considering that the rate of DCF generation was faster when TMPyP was the photosensitizer both in homogeneous media and in PC/CL liposomes, we considered that the presence of lipid bilayers did not affect significantly the quantum yield of $O_2(^1\Delta_g)$ by the cationic porphyrin but increased its stability. Probably, the higher stability of TMPyP bound to lipid bilayers results from the trapping of $O_2(^1\Delta_g)$ by the lipids. This is similar to that was previously described for cytochrome *c* oxidation by $O_2(^1\Delta_g)$ (69) Therefore, the damage on the lipid membranes promoted by photosensitizers is modulated by its affinity to this biological structure that in turn influences the photosensitivity (stability) of the porphyrin and the generation of long-lived $O_2(^1\Delta_g)$. However, the results obtained by using TPPS4 as a photosensitizer indicates that the Type-II mechanism allows a photosensitizer to promote damages on membranes even in the absence of binding affinity. The PC/CL vesicles used in this study are a model of the lipid fraction of the inner mitochondrial membrane. This model does not reproduce active and coupled mitochondria. Effects of transmembrane potential on the oxidative damage of the inner mitochondrial membrane promoted by TMPyP are not contemplated in this study. They require future investigations in more appropriated membrane models, isolated mitochondria and cells.

The next step of these studies will be focused on more specific models, isolated mitochondria and cultured cells. For the latter, the strategy will be the use of different carriers for the photosensitizers leading to specific trafficking mechanisms and targeted organelles. The ultimate objective includes not only the immediate effects and cell death mechanisms modulated by the targeted organelles but also the delayed effects on the expression of genes.

The principal events peculiar to each investigated porphyrin are summarized in Scheme 3.

Acknowledgements—The authors are grateful to FAPESP, CAPES and CNPq for their financial support. The authors thanks also to the Multiusers Central Facilities for the experimental support.

SUPPORTING INFORMATION

Additional Supporting Information may be found in the online version of this article:

Movie S1. GUV changes during irradiation with TPPS4.

Movie S2. GUV changes during irradiation with TMPyP.

REFERENCES

1. Darlenski, R. and J. W. Fluhr (2013) Photodynamic therapy in dermatology: Past, present, and future. *J. Biomed. Opt.* **18**, 061208.
2. Moore, J. V., C. M. L. West and C. Whitehurst (1997) The biology of photodynamic therapy. *Phys. Med. Biol.* **42**, 913–935.
3. Stark, G. (2005) Functional consequences of oxidative membrane damage. *J. Membr. Biol.* **205**, 1–16.
4. Henderson, B. W. and T. J. Dougherty (1992) How does photodynamic therapy work. *Photochem. Photobiol.* **55**, 145–57.
5. Buytaert, E., M. Dewaele and P. Agostinis (2007) Molecular effectors of multiple cell death pathways initiated by photodynamic therapy. *Biochim. Biophys. Acta-Rev. Cancer* **1776**, 86–107.
6. Kübler, A. (2005) Photodynamic therapy. *Med. Laser Appl* **20**, 37–45.
7. Park, J. H., Y. H. Moon, I. S. Bang, Y. C. Kim, S. A. Kim, S. G. Ahn and J. H. Yoon (2010) Antimicrobial effect of photodynamic therapy using a highly pure chlorin e6. *Lasers Med. Sci.* **25**, 705–710.
8. Sharman, W. M., C. M. Allen and J. E. van Lier (1999) Photodynamic therapeutics: Basic principles and clinical applications. *Drug Discovery Today* **4**, 507–517.
9. Konan, Y. N., R. Gurny and E. Allemann (2002) State of the art in the delivery of photosensitizers for photodynamic therapy. *J. Photochem. Photobiol., B* **66**, 89–106.
10. Dolmans, D., D. Fukumura and R. K. Jain (2003) Photodynamic therapy for cancer. *Nat. Rev. Cancer* **3**, 380–387.
11. Choudhary, S., K. Nouri and M. L. Elsaie (2009) Photodynamic therapy in dermatology: A review. *Lasers Med. Sci.* **24**, 971–980.
12. Ravanat, J. L., P. di Mascio, G. R. Martinez, M. H. G. Medeiros and J. Cadet (2000) Singlet oxygen induces oxidation of cellular DNA. *J. Biol. Chem.* **275**, 40601–40604.
13. Bonnett, R., R. D. White, U. J. Winfield and M. C. Berenbaum (1989) Hydroporphyrins of the meso-tetra(hydroxyphenyl)porphyrin series as tumour photosensitizers. *Biochem. J.* **261**, 277–280.
14. Sandell, J. L. and T. C. Zhu (2011) A review of in-vivo optical properties of human tissues and its impact on PDT. *J. Biophotonics* **4**, 773–787.
15. Castano, A. P., T. N. Demidova and M. R. Hamblin (2004) Mechanisms in photodynamic therapy: Part one-photosensitizers, photochemistry and cellular localization. *Photodiagn. Photodyn. Ther.* **1**, 279–293.
16. Dennis, E. J. G. J., D. D. Fukumura and R. K. Jain (2003) Photodynamic therapy for cancer. *Nat. Rev. Cancer* **3**, 380–387.

17. Carvalho, C. B. M., T. J. Brocksom and K. T. Oliveira (2013) Tetrabenzoporphyrins: Synthetic developments and applications. *Chem. Soc. Rev.* **42**, 3302–3317.
18. Robertson, C. A., D. H. Evans and H. Abraharnse (2009) Photodynamic therapy (PDT): A short review on cellular mechanisms and cancer research applications for PDT. *J. Photochem. Photobiol., B* **96**, 1–8.
19. Ben-Dror, S., I. Bronshtein, A. Wiehe, B. Röder, M. O. Senge and B. Erenberg (2006) On the correlation between hydrophobicity, liposome binding and cellular uptake of porphyrin sensitizers. *Photochem. Photobiol.* **82**, 695–701.
20. Berg, K., J. C. Bommer and J. Moan (1989) Evaluation of sulfonated aluminum phthalocyanines for use in photochemotherapy - cellular uptake studies. *Cancer Lett.* **44**, 7–15.
21. Oleinick, N. L. and H. H. Evans (1998) The photobiology of photodynamic therapy: Cellular targets and mechanisms. *Radiation Res.* **150**, S146–S156.
22. Nepomuceno, M. F., M. Tabak and A. E. Vercesi (2002) Opposite effects of Mn(III) and Fe(III) forms of meso-tetrakis(4-N-methyl pyridiniumyl) porphyrins on isolated rat liver mitochondria. *J. Bioenerg. Biomembr.* **34**, 41–47.
23. Inada, N. M., A. R. da Silva, R. A. Jorge, J. Borecky and A. E. Vercesi (2007) Irradiated cationic mesoporphyrin rat liver mitochondria induces larger damage to isolated than the anionic form. *Arch. Biochem. Biophys.* **457**, 217–23.
24. Nantes, I. L., T. Rodrigues, A. C. F. Caires, R. L. O. R. Cunha, F. S. Pessoto, C. H. Yokomizo, J. C. Araujo-Chaves, P. A. Faria, D. P. Santana and C. G. Santos (2011) Specific effects of reactive thiol drugs on mitochondrial bioenergetics. *J. Bioenerg. Biomembr.* **43**, 11–18.
25. Pessoto, F. S., N. M. Inada, M. D. Nepomuceno, A. C. Ruggiero, O. R. Nascimento, A. E. Vercesi and I. L. Nantes (2009) Biological effects of anionic meso-tetrakis (para-sulfonatophenyl) porphyrins modulated by the metal center. Studies in rat liver mitochondria. *Chem. Biol. Inter.* **181**, 400–408.
26. Araujo-Chaves, J. C., F. S. Pessoto, C. H. Yokomizo and I. L. Nantes (2011) Towards the mechanisms involved in the antioxidant action of MnIII [meso-tetrakis(4-N-methyl pyridinium) porphyrin] in mitochondria. *J. Bioenerg. Biomembr.* **43**, 663–671.
27. Patito, I. A., C. Rothmann and Z. Malik (2001) Nuclear transport of photosensitizers during photosensitization and oxidative stress. *Biol. Cell* **93**, 285–291.
28. Brault, D. (1990) Physical chemistry of porphyrins and their interactions with membranes: The importance of pH. *J. Photochem. Photobiol., B* **6**, 79–86.
29. Postigoa, F., M. Moraa, M. A. de Madariagaa, S. Nonellb and M. L. Sagristáa (2004) Incorporation of hydrophobic porphyrins into liposomes: Characterization and structural requirements. *Int. J. Pharm.* **278**, 239–254.
30. Ricchelli, F., G. Jori, S. Gobbo and M. Tronchin (1991) Liposomes as models to study the distribution of porphyrins in cell membranes. *Biochim. Biophys. Acta: Biomembranes* **1065**, 42–48.
31. Ricchelli, F. (1995) Photophysical properties of porphyrins in biological membranes. *J. Photochem. Photobiol., B* **29**, 109–118.
32. Araujo-Chaves, J. C., C. Kawai, A. F. A. A. Melo, K. C. U. Mugnol, O. R. Nascimento, J. T. Arantes, F. N. Crespilho and I. L. Nantes (2013) Interaction and reaction of the antioxidant MnIII [meso-tetrakis(4-N methyi pyridinium) porphyrin] with the apoptosis reporter lipid phosphatidylserine. *Current Phys. Chem.* **3**, 187–198.
33. Skupin-Mrugalska, P., J. Piskorz, T. Goslinski, J. Mielcarek, K. Konopka and N. Düzgüneş (2013) Current status of liposomal porphyrinoid photosensitizers. *Drug Discovery Today* **18**, 776–784.
34. Neto de, D. S., A. Hawe and M. Tabak (2013) Interaction of meso-tetrakis (4-N-methylpyridyl) porphyrin in its free base and as a Zn (II) derivative with large unilamellar phospholipid vesicles. *Eur. Biophy. J.* **42**, 267–279.
35. Almeida, R. D., B. J. Manadas, A. P. Carvalho and C. B. Duarte (2004) Intracellular signaling mechanisms in photodynamic therapy. *Biochim. Biophys. Acta* **1704**, 59–86.
36. Nowis, D., M. Makowski, T. Stokłosa, M. Legat, T. Issat and J. Golab (2005) Direct tumor damage mechanisms of photodynamic therapy. *Acta Biochim. Pol.* **52**, 339–352.
37. Kalyanasundaram, K. and M. Neumann-Spallart (1982) Photophysical and redox properties of water-soluble porphyrins in aqueous-media. *J. Phys. Chem.* **86**, 5163–5169.
38. Riske, K. A., T. Sudbrack, N. L. Archilha, A. F. Uchoa, A. P. Schroder, C. M. Marques, M. S. Baptista and R. Itri (2009) Giant vesicles under oxidative stress induced by a membrane-anchored photosensitizer. *Biophys. J.* **97**, 1362–1370.
39. Haluska, C. K., M. S. Baptista, A. U. Fernandes, A. P. Schroder, C. M. Marques and R. Itri (2012) Photo-activated phase separation in giant vesicles made from different lipid mixtures. *Biochim. Biophys. Acta: Biomembranes* **1818**, 666–672.
40. Mroz, P., J. Bhaumik, D. K. Dogutan, Z. Aly, Z. Kamal, L. Khalid, H. L. Kee, D. F. Bocian, D. Holten and J. S. Lindsey (2009) Imidazole metalloporphyrins as photosensitizers for photodynamic therapy: Role of molecular charge, central metal and hydroxyl radical production. *Cancer Lett.* **282**, 63–76.
41. Rapozzi, V., K. Umezawa and L. E. Xodo (2011) Role of NF B/Snail/RKIP loop in the response of tumor cells to photodynamic therapy. *Laser Surg. Med.* **43**, 575–585.
42. Daghastanli, N. A., R. Itri and M. S. Baptista (2008) Singlet oxygen reacts with 2′,7′-dichlorodihydrofluorescein and contributes to the formation of 2′,7′-dichlorofluorescein. *Photochem. Photobiol.* **84**, 1238–1243.
43. Cano, M., P. Castiller, J. Roales, J. M. Pedrosa, S. Brittle, T. Richardson, A. R. González-Elipec and A. Barrancoc (2010) A transparent TMPyP/TiO_2 composite thin film as an HCl sensitive optochemical gas sensor. *Sensors and Actuators B* **150**, 764–769.
44. Knyukshto, V. N., K. N. Solovyov and G. D. Egorova (1998) Luminescence and structure of the protonated forms of meso-tetraarylporphyrins in solution. *Biospectroscopy* **4**, 121–133.
45. Goto, L. S., C. O. Hokka, J. F. Lima, T. Prieto, A. P. U. Araújo, I. L. Nantes and O. R. J. Nascimento (2012) Structure and pe roxidase activity of ferric Streptomyces clavuligerus orf10-encoded protein P450CLA: UV-visible, CD, MCD and EPR spectroscopic characterization. *J. Braz. Chem. Soc.* **23**, 913–920.
46. Nantes, I. L., N. Durán, S. M. S. Pinto, F. B. Silva, J. S. Souza, N. Isoda, R. A. S. Luz, T. G. Oliveira and V. G. Fernandes (2011) Modulation of the catalytic activity of porphyrins by lipid- and surface- containing nanostructures. *J. Braz. Chem. Soc.* **22**, 1621–1633.
47. Haynie, D. T.. (2008) Binding equilibria, Chapter 7. In *Biological Thermodynamics*, 2nd Edition (Edited by D. T. Haynie), pp 257. Cambridge University Press, Cambridge. ISBN 978-0-521-88446-4.
48. Cantor, C. R. and P. R. Schimmel (1980) *Biophysical chemistry: Part III: The behavior of biological molecules*. W. H. Freeman, San Francisco.
49. Mugnol, K. C. U., M. V. A. Martins, E. C. Nascimento, O. R. Nascimento, F. N. Crespilho, J. T. Arantes and I. L. Nantes (2011) Interaction of Fe(3^+)meso-tetrakis (2,6-dichloro-3-sulfonatophenyl) porphyrin with cationic bilayers: Magnetic switching of the porphyrin and magnetic induction at the interface. *Theor. Chem. Acc.* **130**, 829–837.
50. Braughler, J. M., L. A. Duncan and R. L. Chase (1986) The involvement of iron in lipid peroxidation. Importance of ferric to ferrous ratios in initiation. *J. Biol. Chem.* **261**, 282–289.
51. Oglecka, K., J. Sanborn, A. N. Parikh and R. S. Kraut (2012) Osmotic gradients induce bio-reminiscent morphological transformations in giant unilamellar vesicles. *Front Physiol.* **120**(3), 1–11.
52. Rawls, H. R. and P. J. Vansanten (1970) Possible role for singlet oxygen in the initiation of fatty acid autoxidation. *J. Am. Oil Chem. Soc. A* **47**, 121–125.
53. Adams, G. E. and R. L. Willson (1969) Pulse radiolysis studies on oxidation of organic radicals in aqueous solution. *Trans. Faraday Soc.* **65**, 2981–2987.
54. DeRosa, M. C. and R. J. Crutchley (2002) Photosensitized singlet oxygen and its applications. *Coord. Chem. Rev.* **233**, 351–371.
55. Girotti, A. W. (1990) Photodynamic lipid peroxidation in biological systems. *Photochem. Photobiol.* **51**, 497–509.
56. Magdalena, N., W. Korytowski and A. W. Girotti (2005) Self-sensitized photodegradation of membrane-bound protoporphyrin mediated by chain lipid peroxidation: Inhibition by nitric oxide with sustained singlet oxygen damage. *Photochem. Photobiol.* **81**, 299–305.
57. Foote, C. S. (1991) Definition of type I and type II photosensitized oxidation. *Photochem. Photobiol.* **54**, 659.

58. Musbat, L., H. Weitman and B. Ehrenberg (2013) Azide quenching of singlet oxygen in suspensions of microenvironments of neutral and surface charged liposomes and micelles. *Photochem. Photobiol.* **89**, 253–258.
59. Yoshida, Y., S. Shimakawa, N. Itoh and E. Niki (2003) Action of DCFH and BODIPY as a probe for radical oxidation in hydrophilic and lipophilic domain. *Free Radic. Res.* **37**, 861–872.
60. Rokitskaya, T. I., M. Block, Y. N. Antonenko, E. A. Kotova and P. Poh (2000) Photosensitizer binding to lipid bilayers as a precondition for the photoinactivation of membrane channels. *Biophys. J.* **78**, 2572–2580.
61. Valenzeno, D. P. (1987) Photomodification of biological membranes with emphasis on singlet oxygen mechanisms. *Photochem. Photobiol.* **46**, 147–160.
62. Howe, L. and J. Z. Zhang (1998) The effect of biological substrates on the ultrafast excited-state dynamics of zinc phthalocyanine tetrasulfonate in solution. *J. Photochem. Photobiol. B: Bio.* **67**, 90–96.
63. Krasnovsky, A. A. Jr (1998) Singlet molecular oxygen in photobiochemical systems: IR phosphorescence studies. *Membr. Cell Bio.* **12**, 665–690.
64. Ehrenberg, B., J. L. Anderson and C. S. Foote (1998) Kinetics and yield of singlet oxygen photosensitized by hypericin in organic and biological media. *Photochem. Photobiol.* **68**, 135–140.
65. Valenzeno, D. P. and M. Tarr (1991) Membrane photomodification and its use to study reactive oxygen effects. In *Photochemistry and Photophysics*, Vol. III (Edited by J. F. Rabek), pp. 137–191 CRC Press, Boca Raton, FL.
66. Gensch, T., C. Viappiani and S. E. Braslavsky (1999) Structural volume changes upon photoexcitation of porphyrins: Role of the nitrogen–water interactions. *J. Am. Chem. Soc.* **121**, 10573–10582.
67. Kruk, N. N., B. M. Dzhagarov, V. A. Galievsky, V. S. Chirvony and P. Y. Turpin (1998) Photophysics of the cationic 5, 10, 15, 20-tetrakis(4-N-methylpyridyl)porphyrin bound to DNA, [poly(dA-dT)]2 and [poly(dG-dC)]2: Interaction with molecular oxygen studied by porphyrin triplet–triplet absorption and singlet oxygen luminescence. *J. Photochem. Photobiol. B: Bio.* **42**, 181–190.
68. Redmond, R. W. and J. N. Gamlin (1999) A compilation of singlet oxygen yields from biologically relevant molecules. *Photochem. Photobiol.* **70**, 391–475.
69. Rodrigues, T., L. P. França, C. Kawai, P. A. Faria, K. C. U. Mugnol, F. M. Braga, I. L. S. Tersariol, S. S. Smaili and I. L. Nantes (2007) Protective role of mitochondrial unsaturated lipids on the preservation of the apoptotic ability of cytochrome C exposed to singlet oxygen. *J. Biol. Chem.* **282**, 25577–25587.